A Stepped-Bar Apparatus for Thermal Resistance Measurements

Dakotah R. Thompson

Sameer R. Rao

George W. Woodruff School
of Mechanical Engineering,
Georgia Institute of Technology,
Atlanta, GA 30332

Baratunde A. Cola

George W. Woodruff School
of Mechanical Engineering,
Georgia Institute of Technology,
Atlanta, GA 30332;
School of Materials Science Engineering,
Georgia Institute of Technology,
Atlanta, GA 30332

A stepped-bar apparatus has been designed and constructed to characterize the thermal resistance of materials using steady-state heat transfer techniques. The design of the apparatus is a modification of the ASTM D5470 standard where reference bars of equal cross-sectional area are used to extrapolate surface temperatures and heat flux across a sample of unknown thermal resistance. The design modification involves intentionally oversizing the upper reference bar (URB) of the apparatus to avoid contact area uncertainty due to reference bar misalignment, which is difficult to account for, as well as the high cost that can be associated with equipping the apparatus with precise alignment controls (e.g., pneumatic alignment). Multidimensional heat transfer in the upper reference bar near the sample interface is anticipated using numerical modeling. The resulting nonlinear temperature profile in the upper reference bar is accounted for by fitting a second order regression line through thermocouple readings near the sample interface. The thermal resistances of commercially available thermal gap pads and thermal pastes were measured with the stepped-bar apparatus; the measured values were in good agreement with published results, and exhibited a high degree of reproducibility. The measurement uncertainty of both the standard and stepped-bar apparatus decrease with increased thermocouple precision. Notably, the uncertainty due to reference bar misalignment with the standard apparatus becomes more pronounced as thermocouple precision and the number of thermocouples increases, which suggests that the stepped-bar apparatus would be especially advantageous for enabling accurate, high-precision measurements of very low thermal resistances. [DOI: 10.1115/1.4025116]

Introduction

Because the burgeoning demand for smaller electronics is increasing device and component densities in the semiconductor industry, thermal management of these electronic packages is becoming an increasingly important issue. Thermal interface materials (TIMs) with a high thermal conductance are necessary to cool electronic devices to protect them from overheating. As the power density of electronic devices becomes larger, there is a growing need for higher-performance TIMs and tools to characterize them with the degree of reproducibility demanded in industry. Inaccurately characterized TIMs may lead to failure of electronic devices at an unacceptably high rate. Thus, improved measurement reproducibility will save companies in the electronics industry, which frequently tests TIMs, time and money. As a compounding factor, the advent of new materials has introduced a class of high-performance TIMs [1–5] that are difficult to characterize properly because they have thermal resistances lower than the uncertainty floor of commercially available measurement tools. Research to improve these characterization tools is critical in order for high-performance TIMs to be successfully introduced into the market.

Thermal conductivity and interface resistance of materials are commonly measured using steady-state, 1D heat transfer techniques [6–8]. A standard experimental approach based on ASTM D5470 [9] employs an apparatus that conducts heat longitudinally through two well-characterized reference bars that sandwich a sample of unknown thermal resistance; the thermal resistance of the sample is measured using simple heat conduction equations. There have been several studies in recent years to improve the measurement uncertainty of the standard 1D reference bar apparatus. Savija et al. [10,11] designed and constructed a 1D reference bar apparatus that could characterize commercially available graphite pads with an uncertainty between 2.2% and 13.6%. Kearns [12] developed an apparatus that could measure thermal resistances as low as 3 mm^2 K/W with an uncertainty of 10%. Most notably, Kempers et al. [13] designed a 1D apparatus with a measurement uncertainty of 2.7% for thermal resistances as low as 4.7 mm^2 K/W. Although these studies have effectively reduced the measurement uncertainty of the 1D reference bar apparatus, few improvements regarding reference bar geometry have been considered. Further, the issue of measurement reproducibility has received little attention in the literature, yet is a critical issue in practice when numerous samples must be tested to reach firm conclusions about the data.

The standard approach to calculate the specific thermal resistance of a sample uses Fourier's Law, given in the following equation:

$$R = \frac{\Delta T}{Q} A_c \tag{1}$$

where ΔT is the difference between the upper interface temperature and the lower interface temperature of the sample, Q is the average heat rate through the sample, and A_c is the effective contact area between reference bars and sample. All recent studies of 1D reference bar techniques to measure thermal resistance utilize reference bars of equal cross-sectional area [11–13], which makes reference bars difficult to align with each other and the sample. Any misalignments reduce the effective contact area between the sample and the reference bars ($A_{contact}$). Because such misalignments often go undetected and are difficult to control, significant errors can propagate through the system, making reproducible measurements difficult to achieve.

The values of the interface temperatures and the heat rate in Eq. (1) are calculated by performing a least-squares regression of

Contributed by the Electronic and Photonic Packaging Division of ASME for publication in the Journal of Electronic Packaging. Manuscript received March 15, 2013; final manuscript received June 24, 2013; published online August 13, 2013. Assoc. Editor: Mehmet Arik.

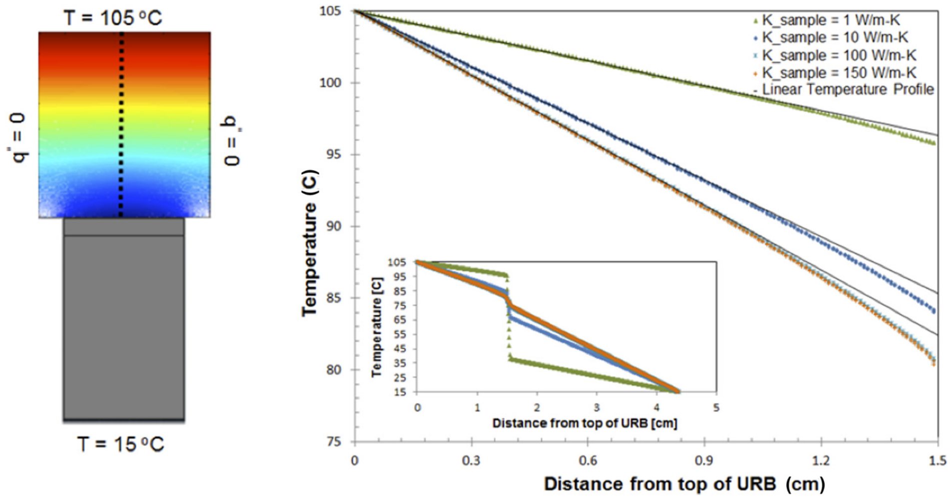

Fig. 1 (*a*) Schematic of model geometry used in 2D heat transfer model. Constant temperature boundary conditions at top of URB and bottom of URB. Zero heat flux boundary conditions on all sides of stepped-bar apparatus. Simulated temperatures in URB recorded along dotted line. (*b*) Simulated center-line (see dotted line in Fig. 1(*a*)) temperature profile in URB of stepped-bar apparatus.

thermocouple readings in each reference bar. The temperature profile through each reference bar in a conventional, well-insulated set-up is linear, allowing heat flux and surface temperatures to be determined by linear regression of thermocouple readings in each reference bar. The slope of the regression line in the upper reference bar is used with simple heat conduction equations to determine the heat rate into the system. Equation (2) gives the specific formulation of the heat conduction equation used to determine the heat rate

$$Q = -kA_{\mathrm{ref}}\frac{dT}{dz} \quad (2)$$

where k is the thermal conductivity of the reference bar, A_{ref} is the cross-sectional area of the reference bar, and dT/dz is the temperature gradient through the reference bar. This procedure is used in the lower reference bar (LRB) to calculate the lower interface temperature at the sample and the heat rate leaving the system. To determine the interface temperature at the top of the sample, this same regression line is extrapolated to the interface.

To improve the reproducibility and accuracy of the 1D reference bar apparatus outlined in the ASTM D5470 standard and described briefly above, we developed a modified "stepped-bar" design with an oversized URB. This modified design allows machining errors and bar misalignments without a reduction in the contact area between the upper reference bar and the sample. This system requires the operator to only align the sample to the LRB rather than aligning the sample to both reference bars, obviating the need for expensive bar alignment mechanisms. As a consequence of this modification, a constriction to heat flow is anticipated between the upper reference bar and the sample, which can be accounted for by the counter measures presented in this study.

Numerical Analysis of Stepped-Bar Design

The temperature profile in the upper reference bar is expected to be nonlinear near the sample interface in the stepped-bar apparatus because of an area constriction from the upper reference bar to the sample. A numerical heat transfer model of the stepped-bar apparatus confirmed that the temperature profile near the sample interface is indeed nonlinear in this design. This 2D heat transfer model was generated in MATLAB and employs a finite-difference method to approximate heat conduction between nodes with a spacing of 0.05 mm. Heat transfer in the stepped-bar design should be modeled as 3D in a rigorous treatment; however, the 2D model used here is sufficient for elucidating the predominate effects of the stepped design on the temperature near the sample interface. A simulated center-line temperature profile in the upper reference bar is shown in Fig. 1.

The 2D MATLAB model of the stepped-bar apparatus used to generate Fig. 1 sets the thermal conductivity of both reference bars to that of Al 2024 ($k = 138$ W/m K). The upper reference bar has a width of 1.4 cm and the lower reference bar has a width of 1 cm. The set point temperatures at the top of the URB and bottom of the LRB were maintained at 105 °C and 15 °C, respectively. Zero heat flux (q'') was maintained as the side boundary condition, which assumes perfectly insulated reference bars. The model was run with a 0.5 mm thick test sample with various thermal conductivity values (K_sample) between 1 and 150 W/m K. These thermal conductivity values correspond to TIM samples with resistances between 500 and 3.3 mm^2 K/W.

Figure 1 shows that the heat spreading effect becomes more pronounced as the thermal conductivity of the sample increases or the resistance of the TIM decreases relative to that of the reference bars. Fitting a linear curve to thermocouple readings in the URB of the stepped-bar apparatus would systematically overestimate the heat rate and produce higher measurement uncertainty because the residual of the regression line would be relatively large.

Based on the numerical analysis, the curve fit of thermocouple readings through the upper reference bar can be divided into a first order fit through the top of the bar and a second order fit through the bottom of the bar to account for nonlinear effects. The first order curve fit in the top of the URB determines the heat rate into the URB. The second order fit in the URB near the sample interface extrapolates the upper interface temperature of the sample. The data in Fig. 1 indicate that the temperature profile in the URB becomes nonlinear within about 5 mm of the sample interface, although this result is only valid for the particular geometry of the stepped-bar set-up presented in this study. The inset of Fig. 1(*b*) shows that the temperature profile in the lower reference bar remains linear, so a single first order curve fit is appropriate to determine the heat rate and interface temperature corresponding to the LRB. The temperature profile through the sample also appears to be linear along the centerline based on this MATLAB model, justifying the validity of Eq. (1) to calculate the sample specific thermal resistance.

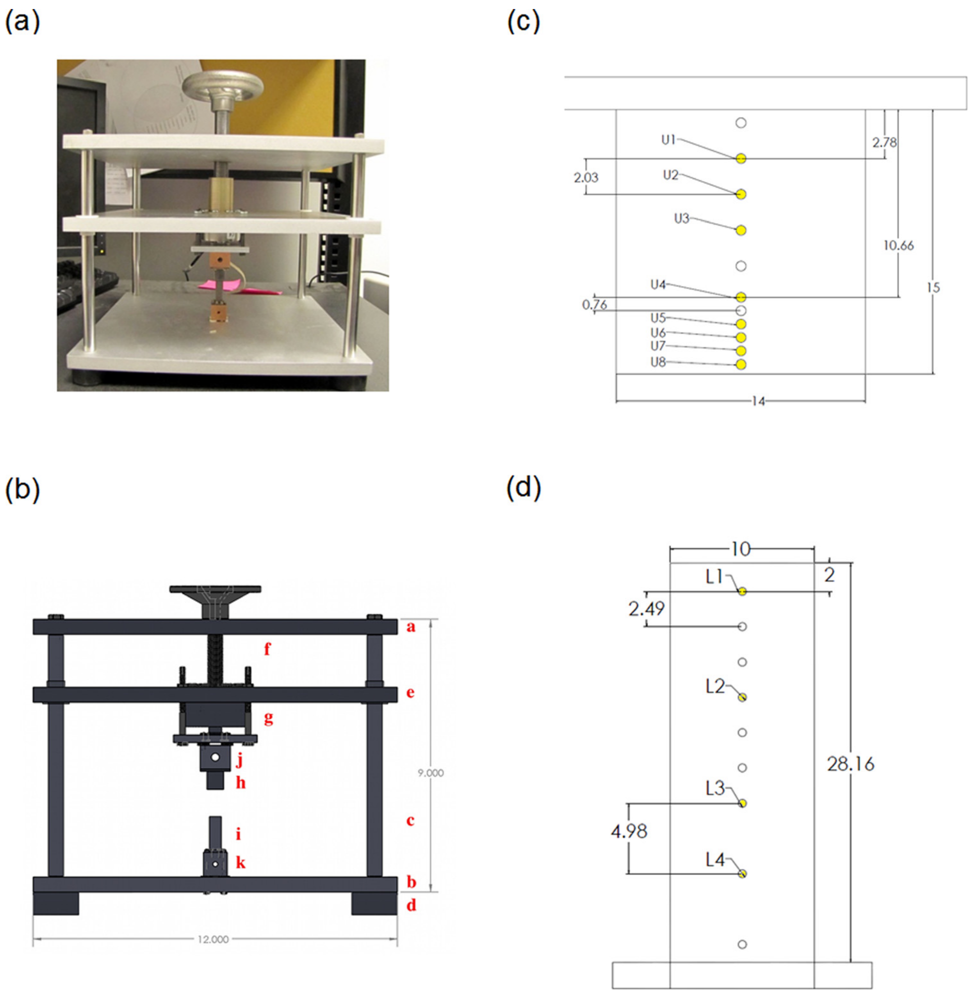

Fig. 2 Stepped-bar thermal measurement apparatus. (*a*) Photograph of apparatus with screw press in place. (*b*) Schematic of apparatus (Two 0.5 in. thick aluminum base plates (*a, b*), each measuring 12 in. × 12 in. Four vertical steel rods (*c*) of 0.5 in. outer diameter. Bottom base plate mounted on rubber feet (*d*) to provide extra stability. Third plate (*e*) mounted in between base plates using Rulon sleeve bearings and the steel rods as guide rails. Assembly connected to mechanical transducer (*f*) comprised of 3/8 in.–12 size acme threaded rod, acme nut and a steel hand wheel. Load cell (*g*) of maximum load 500 N positioned between free plate and thermal test sections (*h, i*) to monitor the pressure being applied to the sample. Cartridge heater (150 W 120 V) embedded in a block (*j*) of oxygen free high conductivity copper (OHFC) and connected to a constant temperature PID controller to maintain the set point and the heat rate through the system. OFHC block (*k*) machined to allow coolant (water) to flow through it. Blocks *j* and *k* serve as the high and low temperature reservoirs, respectively). (*c*) Annotated drawing of URB with thermocouple positions (dimensions in mm). (*d*) Annotated drawing of LRB with thermocouple positions (dimensions in mm).

Stepped-Bar Apparatus Details and Measurement Procedure

The designed and built stepped-bar apparatus is shown in Fig. 2. Two identical sets of stepped reference bars were machined from stainless steel 303 ($k = 15$ W/m K) and aluminum alloy 2024 ($k = 138$ W/m K). According to ASTM standard E1225-09 [14], heat shunting through the insulation around the reference bars occurs when the thermal conductivity of the sample is much less than the thermal conductivity of the reference bars. To avoid heat-shunting errors, the stainless-steel reference bars were necessary to characterize low conductivity or high resistance samples and the aluminum alloy reference bars were required to characterize high conductivity or low resistance samples. As such, the performance of the reference bar apparatus could be characterized for materials over a wide range of thermal conductivity or thermal resistance.

Eight ungrounded T-type thermocouples (Special Limits of Error, ±0.5 K) of diameter 0.020 in. were inserted into the upper reference bar along its length. Four T-type thermocouples of diameter 0.020 in. are inserted into the lower reference bar along its length. A 16-channel temperature recorder (SR 630 Stanford Instruments) was used to acquire the temperature data. We machined a total of 11 thermocouple holes in the upper reference bar and 9 thermocouples in the lower reference bar. These additional holes allow thermocouples to be repositioned and extra thermocouples to be added to the apparatus when necessary. Each thermocouple hole is 0.022 in. in diameter and is machined into the reference bars at a depth equal to half of the bar width. Positions of each thermocouple hole, as well as the relevant features of the set-up are displayed in Fig. 2.

The mechanical transducer, comprised of the threaded rod and steel hand wheel, applies pressure to the sample under test. The use of a mechanical transducer can greatly lower the cost (~50%)

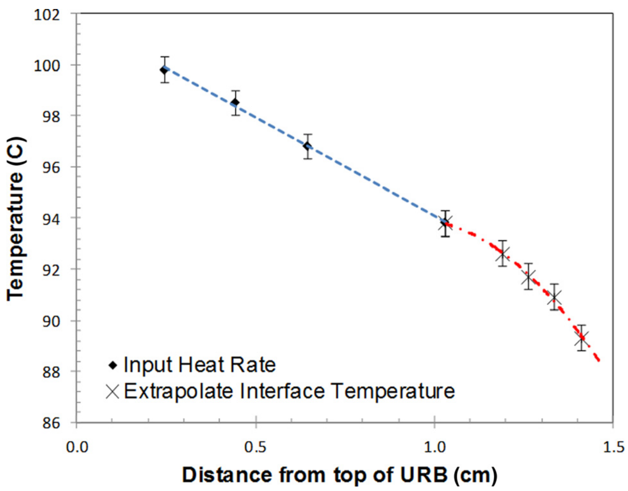

Fig. 3 Curve-fitting procedure in upper reference bar of modified apparatus. The slope of the blue dashed line is used to determine the input heat rate. The red dashed-dot curve is used to extrapolate the interface temperature.

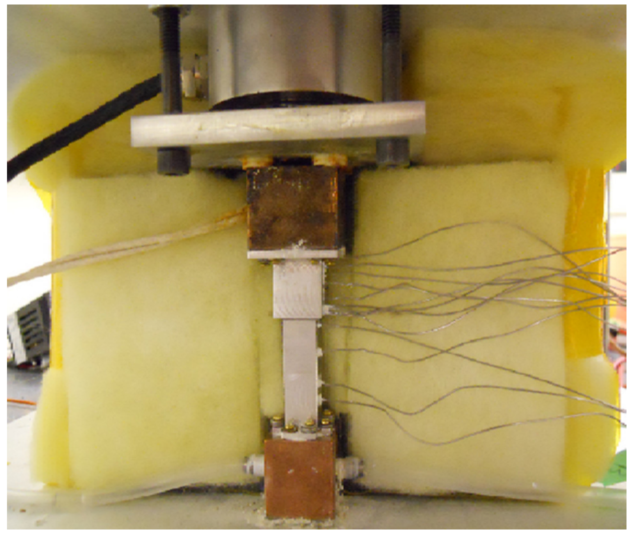

Fig. 4 Cross-sectional view of the custom insulation system surrounding the reference bars. Fiberglass insulation is added to each surface of the nylon foam halves (not seen in the photo). The photo also shows the thermocouples in their measurement positions in each reference bar.

of the entire apparatus in comparison to a stepper motor or pneumatic-based loading system (see section on cost comparison for more details). Because instabilities of the threaded rod introduce imprecision in aligning the upper reference bar with the lower reference bar, the upper reference bar is oversized to ensure that these misalignments do not reduce the contact area of the sample and introduce errors into the thermal resistance measurements. The URB has a square cross-sectional area measuring 1.4 cm to a side. The LRB has a square cross-sectional area measuring 1.0 cm to a side. The URB and LRB are 1.5 cm and 3.0 cm long in the axial direction, respectively.

Heating of the system is delivered by a cylindrical cartridge heater that provides a constant temperature boundary condition at the top of the URB. The heater power is controlled with a constant temperature proportional-integral-derivative (PID) control device. The top thermocouple at the position above U1 in Fig. 2(*c*) is used for the PID control of the cartridge heater so that the upper set point temperature remains constant during steady-state operation. The cooling of the heat sink below the LRB is realized by the use of a constant temperature coolant recirculator.

The heat rate into the URB is measured by fitting a first order curve through four thermocouple readings corresponding to thermocouple positions U1, U2, U3, and U4. The slope of this line gives the temperature gradient along the centerline of the URB. Knowledge of the reference bar thermal conductivity and cross-sectional area are used with Equation (2) to determine the heat rate into the URB. Similarly, a first order curve is fit through the thermocouple readings in the LRB, corresponding to thermocouple positions L1, L2, L3, and L4, to measure the heat rate out of the sample. This first order fit is also used to extrapolate the lower interface temperature of the sample.

The upper interface temperature is calculated by fitting a second order curve through the thermocouple readings in the URB to account for heat constriction. Specifically, the second order curve is fit through thermocouples corresponding to thermocouple positions U4, U5, U6, U7, and U8 and the interface temperature is extrapolated from this curve. This curve-fitting procedure in the URB is shown graphically in Fig. 3 for a representative measurement.

The error bars in Fig. 3 depict the uncertainties of the T-type thermocouples as well as the uncertainties in their positions. The second order curve fit was applied to the nonlinear portion of the temperature profile in the URB, which was accurately predicted to be within 5 mm of the sample interface by the numerical analysis described previously (Fig. 1).

Both reference bars were well-insulated on each side with a custom insulation system, shown in Fig. 4. The insulation system is comprised of two halves of a nylon foam block (not shown) that enclose the reference bars. The reference bars are surrounded by 3.5 in. of nylon foam on each side. Additional layers of fiberglass insulation were added to each surface of the nylon foam halves to provide additional insulation.

Several commercially available samples were characterized in the stepped-bar apparatus using aluminum alloy Al-2024 ($k = 138$ W/m K) reference bars. The thermal conductivity of these Al-2024 reference bars was measured using a HotDisk thermal conductivity analyzer. The faces of the reference bars were highly polished, with an average roughness of 0.5 μm and a flatness between 0.127 and 0.254 μm. A high set point temperature was maintained at 105 °C and the chiller set point temperature was maintained at 15 °C for all measurements. Samples were measured under applied pressures ranging from 50 kPa to 400 kPa. Two different thermal pastes were characterized: Arctic Silver 5 and Ceramique. A small amount of spacer-grade, soda lime glass microspheres (22–25 μm) from Cospheric was added to these pastes to maintain a constant bond line thickness over the range of applied pressures. It was assumed that these spacer beads did not significantly affect the measured thermal resistance values because they comprise only a small volume fraction of the paste under test.

We also tested the repeatability of the stepped-bar apparatus with stainless steel SS-303 ($k = 15$ W/m K) reference bars by measuring a sample of TC100 thermal gap pad manufactured by Stockwell Elastomerics. The manufacturer-specified value of the specific thermal resistance across the TC100 sample of thickness 1.575 mm is 12.1 cm^2 K/W [15]. The testing conditions specified by the manufacturer are as follows: testing pressure is 690 kPa and mean stack temperature is 100 °C. We measured the TC100 sample in the stepped-bar apparatus at the manufacturer-specified testing pressure. The chiller set point temperature was 15 °C. Measurements were taken with upper set point temperatures of 70 °C, 140 °C, 160 °C, and 190 °C. For each measurement, the sample was removed from the apparatus and reinserted to account for operator error in aligning the sample to the LRB.

Measurement Results

Figure 5 reveals thermal resistance measurements of the thermal pastes to be slightly pressure dependent for each sample. A

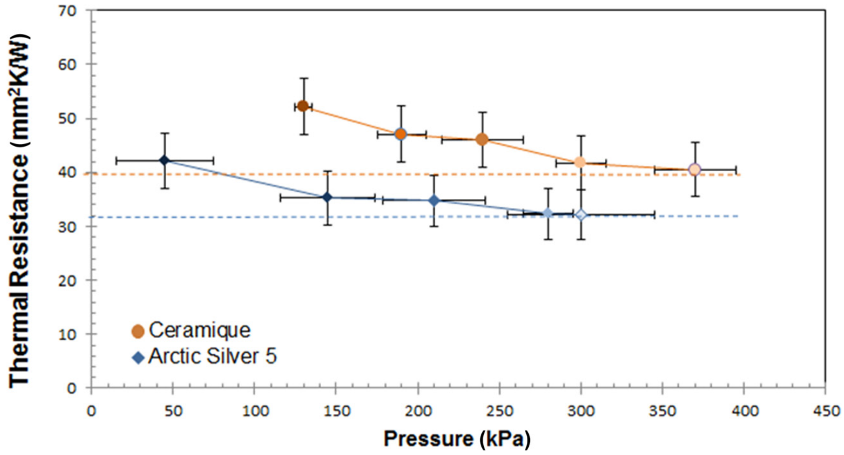

Fig. 5 Measured thermal resistance of commercially available thermal paste. The dashed orange and blue lines estimate the lower bounds of the measured thermal resistances for Ceramique and Arctic Silver 5, which occur at high pressures.

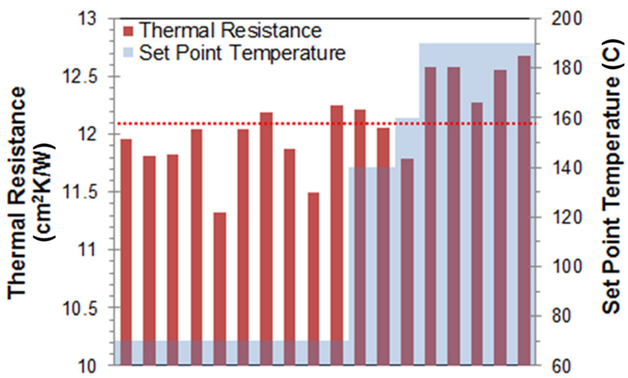

Fig. 6 Frequency histogram of 18 independent thermal resistance measurements (red) of TC100 thermal interface material. The sample was removed and reloaded in the system after each measurement. Manufacturer-specified thermal resistance of TC100 sample was 12.12 cm^2 K/W. The dotted red line indicates the average value of the thermal resistance measurements. Also shown is the upper set point temperature (blue shaded region) used in each measurement.

minimum thermal resistance of 32 mm^2 K/W ($\pm$14.7%) was measured for Arctic Silver 5 at an applied pressure of 300 kPa. This result agrees closely with a similar study by NREL in 2008 [4], which measures the thermal resistance for Arctic Silver 5 with a bond line thickness of 23.5 μm to be 30.9 mm^2 K/W. The NREL study used an experimental apparatus based on ASTM D5470 with reference bars polished to 0.5 μm and test pressures between 170 and 340 kPa.

Figure 6 shows the frequency histogram for all measurements of the TC100 gap pad using the stepped-bar apparatus with stainless-steel reference bars. The average specific thermal resistance measurement was approximately 12.09 cm^2 K/W. The standard deviation of the eighteen measurements was 0.38 cm^2 K/W. A confidence interval based on the student's T distribution suggests that 95% of all measurements of the TC100 gap pad fall within 6.4% of the mean value. These results imply good repeatability of the stepped-bar apparatus under these testing conditions. Likewise, the manufacturer-specified thermal resistance value of 12.12 cm^2 K/W falls within this 95% confidence interval, suggesting excellent measurement accuracy.

There is a slight skew of the histogram in Fig. 6. This skew is the result of heat loss from the apparatus at the higher set point temperatures. Heat losses tend to increase the value of the thermal resistance measurement. These results suggest that there is an important trade-off to be made when selecting testing conditions. Using higher set point temperatures reduces measurement uncertainty because it generates larger temperature drops between adjacent thermocouples. However, a higher set point temperature also increases heat losses, which adversely affects measurement accuracy.

Table 1 Uncertainty of measured quantities

Measured quantity	Uncertainty
Temperature	$\pm$0.5 K (T-type)
Thermocouple position	$\pm$25.4 μm
Reference bar thermal conductivity (Al 2024)	$\pm$1.5 W/m K

Uncertainty Analysis

A rigorous error analysis was performed to estimate how the uncertainties in each measured value propagate through the specific thermal resistance measurement of the stepped-bar apparatus. Table 1 lists the uncertainty of each measured quantity.

The uncertainty of each thermocouple position is equal to the difference between the radius of the hole and the radius of the thermocouple [13]. The uncertainty of the temperature measurement is based on the Special Limits of Error for the T-type thermocouples [16]. The error contribution from the SR 630 thermocouple reader was assumed to be negligible. The uncertainty in the thermal conductivity measurement of the reference bars was determined by the precision of the HotDisk thermal conductivity analyzer [17].

The overall uncertainty of the specific thermal resistance measurement is derived from the Kline and McClintock method [18], given generically by the following equation:

$$U_z = \sqrt{\sum_{i=1}^{n}\left[\frac{\partial Z}{\partial x_i}U_i\right]^2} \tag{3}$$

where U_i is the uncertainty of each measured quantity x_i. Using Eq. (1) to calculate the specific thermal resistance results in a formulation of Kline and McClintock given by

$$U_{\mathrm{R}} = \sqrt{\left[\frac{A_c}{Q}U_{\Delta T}\right]^2 + \left[\frac{\Delta T A_c}{Q^2}U_Q\right]^2 + \left[\frac{\Delta T}{Q}U_{A_c}\right]^2} \tag{4}$$

where A_c is the effective contact area between the sample and the reference bars. The value of ΔT is the difference between the top interface temperature and bottom interface temperature. The value of $U_{\Delta T}$ was calculated using

$$U_{\Delta T} = \sqrt{\left[U_{T_{\text{int,top}}}\right]^2 + \left[U_{T_{\text{int,bot}}}\right]^2} \tag{5}$$

where $T_{\text{int,top}}$ is the top interface temperature of the sample and $T_{\text{int,bot}}$ is the bottom interface temperature of the sample. The value of Q was calculated as the average value of the heat rate through the URB and LRB. The uncertainty U_Q was calculated using

$$U_Q = \sqrt{\left[0.5U_{Q_{\text{top}}}\right]^2 + \left[0.5U_{Q_{\text{bot}}}\right]^2} \tag{6}$$

where $U_{Q_{\text{top}}}$ is the uncertainty of the heat rate in the upper reference bar and $U_{Q_{\text{bot}}}$ is the uncertainty of the heat rate in the lower reference bar. Recall that the heat rate through each reference bar is calculated using simple heat conduction equations. Equations (7) and (8) show how the uncertainty of the heat rate through each reference bar is calculated

$$U_{Q_{\text{top}}} = \sqrt{\left[kA_{\text{top}}U_{G_{\text{top}}}\right]^2 + \left[A_{\text{top}}G_{\text{top}}U_k\right]^2 + \left[kG_{\text{top}}U_{A_{\text{top}}}\right]^2} \tag{7}$$

$$U_{Q_{\text{bot}}} = \sqrt{\left[kA_{\text{bot}}U_{G_{\text{bot}}}\right]^2 + \left[A_{\text{bot}}G_{\text{bot}}U_k\right]^2 + \left[kG_{\text{bot}}U_{A_{\text{bot}}}\right]^2} \tag{8}$$

where k is the thermal conductivity of the reference bar, A is the cross-sectional area of the reference bar, and G is the temperature gradient through the reference bar. Subscripts top and bot refer to the upper and lower reference bars, respectively. Recall that we obtain the values of $T_{\text{int,top}}$, $T_{\text{int,bot}}$, G_{top}, and G_{bot} by performing a least-squares regression of the thermocouple readings in each reference bar. The uncertainty in these measurements reflects the error in the thermocouple readings and thermocouple placement, as well as the statistical error related to the residual of the least-squares regression.

A Monte Carlo analysis of the least-squares regression performed in each reference bar is used to determine the uncertainties $U_{T_{\text{int,top}}}$, $U_{T_{\text{int,bot}}}$, $U_{G,\text{top}}$, and $U_{G,\text{bot}}$. The Monte Carlo analysis involves perturbing experimental thermocouple readings and thermocouple positions by the standard uncertainty of each measurement. Each thermocouple reading is perturbed by a T_{error} term. The T_{error} term is generated from a random normal distribution with a standard deviation of 0.25 K to reflect the uncertainty of the T-type thermocouple readings [16]: we assume that the special limits of error of $\pm$ 0.5 K for T-type thermocouples is based on a 95% confidence interval or twice the standard deviation. Likewise, thermocouple positions are randomly perturbed by a term generated from a random distribution with maximum values of $\pm 25.4\ \mu$m. Thus, we generate multiple sets of perturbed data and perform a least-squares regression to each one of these perturbed data sets. The standard uncertainties $U_{T_{\text{int,top}}}$, $U_{T_{\text{int,bot}}}$, $U_{G,\text{top}}$, and $U_{G,\text{top}}$ are then calculated by taking the standard deviation of the parameters of the entire set of curve fits. The standard deviations of the slopes of the linear regression in the URB and LRB determine the values $U_{G,\text{top}}$ and $U_{G,\text{top}}$, respectively. The standard deviations of the extrapolated temperatures of the second order curve fit in the URB and the linear curve fit in the LRB determine the values of $U_{T_{\text{int,top}}}$ and $U_{T_{\text{int,bot}}}$, respectively.

A 2D heat transfer model of a standard reference bar apparatus was developed in MATLAB to compare the uncertainty of the stepped-bar apparatus to the standard apparatus using the analysis technique discussed above. The model was used to simulate the temperature profile through reference bars of equal cross-sectional area with varying degrees of reference bar misalignment. Similar to the model used to analyze the stepped-bar design, this finite-difference model used nodes with a spacing of 0.05 mm, and considered all sides to be insulated perfectly. The model also fixes the sample and LRB in perfect alignment so that the contact area is only reduced because of misalignment of the URB. The same heater and heat sink set point temperatures used in the 2D analysis of the stepped-bar design were used here. Using these boundary conditions, the numerical model generates virtual thermocouple readings that have the same placement as the thermocouples used in our actual stepped-bar apparatus. As a result, the measurement uncertainty of the stepped-bar apparatus can be compared to that of a standard apparatus with the same number, placement, and precision of thermocouples.

To directly observe the effects of reference bar misalignment without considering machining errors, we set the uncertainty U_A of the reference bar cross-sectional area to zero for both the stepped-bar apparatus and simulated standard apparatus. For the standard apparatus, we estimate the uncertainty U_{A_c} of the sample contact area, which results from misalignment of the URB, using

$$U_{A_c} = \frac{1}{2}A_{\text{bot}}\chi \tag{9}$$

where χ is the percent reduction in the effective heat transfer area of the sample due to misalignment of the URB. Figure 7(*a*) depicts a probable geometry for misalignment of the URB, which includes lateral translation in both directions as well as rotational misalignment. For mathematical simplicity, we developed a model that only considers the lateral misalignment of the reference bar in one direction as depicted in Fig. 7(*b*).

The contact area in perfect reference bar alignment is defined as

$$A_c = xy \tag{10}$$

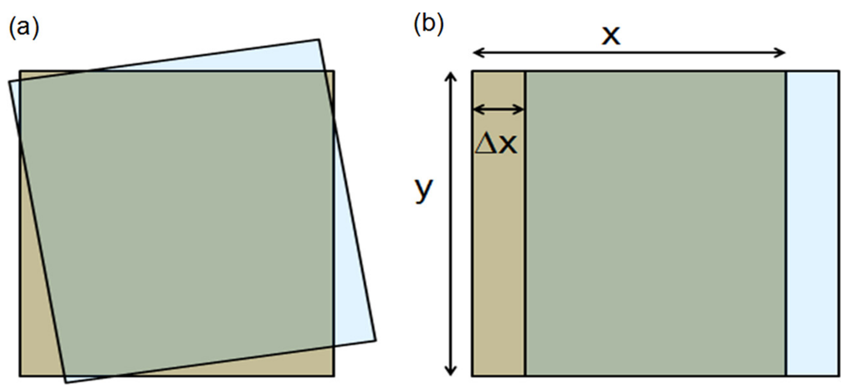

Fig. 7 (*a*) Top-view of lateral and rotational misalignment of upper reference bar. (*b*) Top-view of 1D misalignment of upper reference bar.

The uncertainty in the contact area is given as

$$U_{A_c} = \sqrt{(yU_x)^2 + (xU_y)^2} \tag{11}$$

It is apparent from Fig. 7(*b*) that the value of U_y is zero. Based on a flat distribution, the value of U_x can be estimated as $\Delta x/2$. Thus, the expression for the contact area uncertainty is given as

$$U_{A_c} = \frac{1}{2} y \Delta x \tag{12}$$

The value of Δx can be expressed in terms of the percent misalignment of the upper reference bar to the sample as

$$\chi = \frac{xy - y(x - \Delta x)}{xy} \tag{13}$$

where χ is the percent contact area reduction due to misalignment. After cancelations, Eq. (13) reduces to

$$\chi = \frac{\Delta x}{x} \tag{14}$$

Equation (9) is recovered by substituting Eq. (14) into Eq. (12). It is important to note that this estimation of the contact area uncertainty only considers the special case of 1D misalignment. In reality, reference bar misalignment can arise from lateral translation in either or both directions, as well as rotational misalignment as shown in Fig. 7(*a*). However, we do not undertake a more rigorous analysis of the contact area uncertainty for all cases of reference bar misalignment in this work because establishing the percent reduction in contact area based on 1D misalignment is sufficient to illustrate the effects of misalignment on measurement uncertainty.

The measurement uncertainty for the stepped-bar apparatus was calculated for various samples, including the graphite pad HT 1220 from GrafTech ($k = 10$ W/m K, thickness = 0.51 mm) [19]. The measurement uncertainty of the standard reference bar apparatus for the HT 1220 was then calculated using the numerical model. In the model, the set point temperatures at the top of the URB and bottom of the LRB were 105 °C and 15 °C, respectively. The percent misalignment of the URB with respect to the LRB and sample was then varied from 0% to 18% and simulated thermocouple readings were generated. Thus, the uncertainty of a standard apparatus could be directly compared to the experimental uncertainty of our stepped-bar apparatus measuring the same graphite pad (HT 1220). The results of the uncertainty analysis comparing the stepped-bar apparatus to a standard apparatus are shown in Fig. 8.

In Fig. 8, the solid black line represents the measurement uncertainty of the stepped-bar apparatus when T-type thermocouples (±0.5 K) are used. The black dashed line represents the measurement uncertainty of the stepped-bar apparatus when high-precision thermistors (±0.001 K) are used. Similarly, the solid and dashed red lines correspond to measurement uncertainties for the standard apparatus with T-type thermocouples and high-precision thermistors, respectively: the number and placement of these temperature probes is identical to that of the stepped-bar apparatus. The uncertainty of the ASTM D5470-06 standard reference bar apparatus is plotted in blue. ASTM D5470-06 requires only two temperature probes in each reference bar[3]. From Fig. 8, it is clear that the number of thermocouples in each reference bar has a smaller effect on the measurement uncertainty when more precise temperature probes are used.

We assume that misalignment of the reference bars does not affect the measurement uncertainty of the stepped-bar apparatus since the contact area of the sample is not reduced. On the other hand, the measurement uncertainty of the standard apparatus increases nonlinearly with reference bar misalignment. Figure 8 suggests that the relative contribution of the reference bar

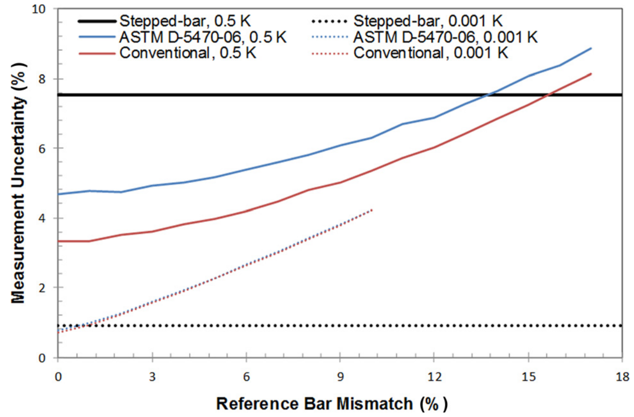

Fig. 8 Comparison of measurement uncertainty for standard and stepped-bar apparatus with Al 2024 meter bars and a graphite pad TIM. Solid lines and dotted lines represent measurement uncertainties when 0.5 K and 0.001 K temperature probes are used, respectively. ASTM D-5470-06 and conventional reference bar curves overlap for high-precision (0.001 K) thermal probes.

misalignment to the overall measurement uncertainty of the standard apparatus increases as the temperature probes used become more precise. For example, Kempers et al. [13] use ±0.001 K resolution thermistors to take highly precise thermal conductivity measurements. With thermistors such as these, the measurement uncertainty of a standard apparatus is greater than that of the stepped-bar apparatus if reference bars are misaligned by 1% or more. Aligning equal-area reference bars with a mismatch less than 1% may be difficult to achieve without the aid of expensive pneumatic alignment mechanisms and in situ metrology to verify alignment. Thus, operators that require highly precise thermal resistance measurements may be able to decrease the uncertainty of their measurements while also saving money on equipment to align the reference bars precisely when the stepped-bar approach is used.

An analysis of the statistical uncertainty in the least-squares regression for each apparatus explains why the measurement uncertainty for the stepped-bar apparatus is greater than that of a perfectly aligned conventional apparatus. Recall that least-squares regression involves fitting a curve of a certain order through a number of data points. The degree of freedom of this regression is given by

$$\gamma = n - O \tag{15}$$

where γ is the degree of freedom, n is the number of data points, and O is the number of parameters in the regression line. The stepped-bar apparatus fits a first order curve through the top four thermocouples and a second order curve through the bottom five thermocouples in the URB. Each of these curve fits has two degrees of freedom. However, a standard apparatus with eight thermocouples in the URB employs a first order fit that has six degrees of freedom. The statistical uncertainty of the parameters of a best-fit equation increases as the degrees of freedom parameter decreases [20]. As a result, the uncertainty of the heat rate and upper interface temperature are greater for the stepped-bar apparatus than for the conventional apparatus because the least-squares regression for the stepped-bar apparatus has fewer degrees of freedom than that of the conventional apparatus with the same number of thermocouples. ASTM D5470-06 requires the use of only two temperature probes in each reference bar [9], which results in zero degrees of freedom in each curve fit in the URB and LRB. Therefore, Fig. 8 shows that the uncertainty curve for the conventional apparatus with T-type thermocouples shifts upward by a significant amount if the ASTM D5470-06 standard is used. As a result, the measurement uncertainty of the stepped-bar apparatus compares more favorably to that of an apparatus adhering to ASTM standards when thermocouple precision is relatively low.

Table 2 Cost-comparison between reference bar set-ups

Manufacturer	Total cost ($)
Our stepped-bar apparatus	9681
Culham [21]	23,785
Huafeng instrument [22]	9000–13,000

Cost of Stepped-Bar Versus Standard Apparatus

The cost of a reference bar apparatus is an important consideration in industry and academic research settings. In order for the stepped-bar apparatus to achieve the same uncertainty as that of a conventional apparatus, more temperature probes are required. Each additional temperature probe increases the cost of the apparatus. However, the stepped-bar apparatus offsets this extra expense because it utilizes an inexpensive mechanical transducer instead of more costly pneumatic-based alignment mechanisms that are required to precisely align reference bars of equal cross-section area. A parts list for the stepped-bar apparatus is tabulated in the Appendix. Table 2 compares the cost of our stepped-bar apparatus to several commercially available standard reference bar set-ups.

Conclusions

This study demonstrates that a modified reference bar apparatus with an oversized upper reference bar can achieve more precise thermal resistance measurements than a standard apparatus with equal cross-sectional area reference bars. Misalignment of equal-area reference bars tends to decrease the contact area of the sample without the operator knowing. Thus, reference bar misalignment propagates error through the thermal resistance measurement of a standard 1D reference bar apparatus. Because the modified apparatus employs an oversized upper reference bar, it eliminates this source of misalignment error, and enables thermal resistance measurements with high reproducibility as a result. The measurement uncertainty of the modified apparatus is less than that of a standard apparatus for reference bar misalignments greater than 1% when highly precise (± 0.001 K) thermal probes are employed. This fact suggests that a stepped-bar apparatus may be appropriate when highly precise thermal resistance measurements are desired. This study also reveals that the placement and number of thermocouples in each reference bar are crucial parameters that greatly affect the measurement uncertainty of the reference bar apparatus.

Acknowledgment

This work was partially supported by National Science Foundation Award No. CBET 1055479 and the NSF Pre-Teaching Summer Undergraduate Research Experience program at Georgia Tech.

References

[1] Cola, B. A., Xu, J., and Fisher, T. S., 2009, "Contact Mechanics and Thermal Conductance of Carbon Nanotube Array Thermal Interfaces," Int. J. Heat Mass Transfer, **52**, pp. 3490–3503.
[2] Harris, D. K., Palkar, A., and Wonacott, G., 2010, "An Experimental Investigation in the Performance of Water-Filled Silicon Microheat Pipe Arrays," ASME J. Electron. Packag., **132**(2), p. 021005.
[3] Huang, H., Liu, C. H., Wu, Y., and Fan, S., 2005, "Aligned Carbon Nanotube Composite Films for Thermal Management," Adv. Mater., **17**(13), pp. 1652–1656.
[4] Narumanchi, S., Mihalic, M., and Kelly, K., 2008, "Thermal Interface Materials for Power Electronics Applications," Itherm 2008, Orlando, FL, May 28–31, Paper No. NREL/CP-540-42972.
[5] Xu, J., and Fisher, T. S., 2005, "Enhancement of Thermal Interface Materials With Carbon Nanotube Arrays," Int. J. Heat Mass Transfer, **49**, pp. 1658–1666.
[6] Gwinn, J. P., and Webb, R. L., 2003, "Performance and Testing of Thermal Interface Materials," Microelectron. J., **34**(3), pp. 215–222.
[7] Khandelwal, M., and Mench, M. M., 2006, "Direct Measurement of Through-Plane Thermal Conductivity and Contact Resistance in Fuel Cell Materials," J. Power Sources, **161**, pp. 1106–1115.
[8] Liao, P., Hua, Z. K., Liao, Y. C., and Zhang, J. H., 2010, "A Novel Thermal Conductivity Meter for Thermal Interface Materials in Optoelectronic Device," 11th International Conference on Electronic Packaging Technology and High Density Packaging (ICEPT-HDP), Xi'an, China, August 16–19, pp. 889–892.
[9] ATSM, 2006, "Standard Test Method for Thermal Transmission Properties of Thermally Conductive Electrical Insulating Materials," D5470, ASTM International, West Conshohocken, PA.
[10] Savija, I., Culham, J. R., and Yovanovich, M. M., "Effective Thermophysical Properties of Thermal Interface Materials: Part I—Definitions and Models," Proceedings of ASME International Electronic Packaging Technical Conference and Exhibition, Maui, HI, July 6–11, ASME Paper No. IPACK2003-35088, pp. 189–200.
[11] Savija, I., Culham, J. R., and Yovanovich, M. M., "Effective Thermophysical Properties of Thermal Interface Materials: Part II—Experiments and Data," Proceedings of International Electronic Packaging Technical Conference and Exhibition, Maui, HI, July 6–11, ASME Paper No. IPACK2003-35264, pp. 567–573.
[12] Kearns, D., 2003, "Improving Accuracy and Flexibility of ASTM D 5470 for High Performance Thermal Interface Materials," 19th IEEE Semiconductor Thermal Measurement and Management Symposium, San Jose, CA, March 11–13, pp. 129–133.
[13] Kempers, R., Kolodner, P., Lyons, A., and Robinson, A. J., 2009, "A High-Precision Apparatus for the Characterization of Thermal Interface Materials," Rev. Sci. Instrum., **80**, p. 095111.
[14] ASTM, 2004, "Standard Test Method for Thermal Conductivity of Solids by Means of the Guarded-Comparative-Longitudinal Heat Flow Technique," E1225, ASTM International, West Conshohocken, PA.
[15] Stockwell Elastomerics, 2012, "Thermally Conductive Silicon Rubber Heat Transfer Pads and Gaskets From Gap Filling Compounds," Stockwell Elastomerics, Inc., Philadelphia, PA, http://www.stockwell.com/data_sheets/thermal/se200_thermal_mgmt_products.pdf
[16] ASTM, 2011, "Standard Specification and Temperature-Electromotive Force (emf) Tables for Standardized Thermocouples," E230/E230M-11, ASTM International, West Conshohocken, PA.
[17] Hot Disk, 2012, "TPS 1500," Hot Disk AB, Gothenburg, Sweden, http://www.hotdiskinstruments.com/products/instruments/tps-1500.html
[18] Kline, S. J., and McClintock, F. A., 1953, "Describing Uncertainties in Single-Sample Experiments," Mech. Eng., **75**(1), pp. 3–8.
[19] GrafTech, 2012, "HITHERM Thermal Interface Materials Technical Data Sheet 318," GraphTech International, Parma, OH, http://graftechaet.com/getattachment/a98eb932-9a95-419f-82e5-9d7683b6b67b/eGRAF%C2%AE-HITHERM%E2%84%A2-Typical-Properties.aspx
[20] Bowker, A. L., and Lieberman, G. J., 1972, *Engineering Statistics*, 2nd ed., Prentice-Hall, Englewood Cliffs, NJ.
[21] Culham, J. R., Teertstra, P., Savija, I., and Yovanovich, M. M., 2002, "Design, Assembly and Commissioning of a Test Apparatus for Characterizing Thermal Interface Materials," Eighth Intersociety Conference on Thermal and Thermomechanical Phenomena in Electronic Systems (ITHERM 2002), San Diego, CA, June 1, pp. 128–135.
[22] Hunan Zhenhua Analysis Instrument Co., 2013, "DRX-I-PB/PC Thermal Conductivity Tester (Guarded Hot Plate Testing System)," http://hfyq.en.alibaba.com/product/553015923-209348254/DRX_I_PB_PC_Thermal_Conductivity_Tester_Guarded_hot_plate_testing_system_.html

Erratum Notice

This paper has been modified since being posted online. The DOI of the published erratum is: 10.1115/1.4025800

The following Appendix on the next page has been incorporated into this version of the paper.

Appendix

Table 3 Parts list for stepped-bar apparatus

Part name	Supplier	Part ID	Unit cost ($)	No. of units	Total cost ($)
Machining components					
Cast iron hand wheel	McMaster Carr	6025K37	12.8	1	12.8
ACME threaded rod	McMaster Carr	99030A277	56.25	1	56.25
ACME round nut	McMaster Carr	95072A371	54.63	1	54.63
ACME round nut mounting flange	McMaster Carr	95082A643	32.58	1	32.58
Ceramic washer	McMaster Carr	94610A215	3.14	1	3.14
Shaft/support rod	McMaster Carr	6649K101	43.32	4	173.28
Sleeve bearing rulon	McMaster Carr	6371K119	27.44	1	27.44
Rubber feet	McMaster Carr	9540K36	14.48	1	14.48
Copper alloy 110 block	McMaster Carr	89275K54	206.33	1	206.33
Aluminum alloy 2024 block	McMaster Carr	86895K231	36.34	1	36.34
Pressure application					
Load cell	Omega Engineering	LCM305-500N	480	1	480
Digital strain gage meter	Omega Engineering	DPiS32	195	1	195
Temperature recording					
Thermocouples	Omega Engineering	TJ36-CPSS-020U-6	33	13	386.10
16 channel reader	Stanford Instruments	SR 630	1495	1	1495
Heater/chiller					
Cartridge heater	Omega Engineering	CIR-1014/120	47	2	94
Process control	Omega Engineering	CN 8201-DC1-C2	359	1	359
Heat sink	Omega Engineering	FHS-6	21	1	21
Fuse holder	Omega Engineering	FB-1	20	2	40
Fuse	Omega Engineering	KAX-10	30	2	60
Solid state relay	Omega Engineering	SSR L240DC10	21	1	21
Chiller	VWR scientific	13271-110	3605.91	1	3605.91
DAQ and communication					
NI GPIB-USB-HS	National Instruments	778927-01	549	1	549
X2 GPIB cable	National Instruments	763061-005	75	1	75
X2 GPIB cable	National Instruments	763061-02	90	1	90
Miscellaneous					
Nylon foam insulation	McMaster Carr	3623K64	5.16	7	36.12
Flexible fiberglass insulation	McMaster Carr	4478K1	6.28	1	6.28
Machining costs (meter bars)	—	—	1550	—	1550
				Grand total	$9681